



# An Immobilized Enzyme Reactor for Spatiotemporal Control over Reaction Products

Jennifer Grant, Justin A. Modica, Juliet Roll, Paul Perkovich, and Milan Mrksich\*

This paper describes a microfluidic chip wherein the position and order of two immobilized enzymes affects the type and quantity of reaction products in the flowing fluid. Assembly of the chip is based on a self-assembled monolayer presenting two orthogonal covalent capture ligands that immobilize their respective fusion enzyme. A thiol-tagged substrate is flowed over a region presenting the first enzyme—which generates a product that is efficiently transferred to the second enzyme—and the second enzyme's product binds to an adjacent thiol capture site on the chip. The amount of the three possible reaction products is quantified directly on the chip using self-assembled monolayers for matrix-assisted laser desorption/ionization mass spectrometry, revealing that the same microsystem can be spatiotemporally arranged to produce different products depending on the device design. This work allows for optimizing multistep biochemical transformations in favor of a desired product using a facile reaction and analytical format.

## 1. Introduction

Enzymes are responsible for almost every metabolic transformation in the living cell. Therefore, enzyme networks must perform robustly despite competing reactions, flux imbalances, and accumulation of toxic intermediates. To overcome these challenges, cells often organize metabolic reactions spatially and temporally using membrane-bound enzymes and highly ordered enzyme complexes. In this manner, metabolic processes involving multiple enzymatic transformations efficiently channel metabolites between active sites to effectively control the reaction products and their rates of formation. One characteristic of a spatiotemporally organized reaction network is that the same set of enzymes can generate unique reaction products depending on the order of enzyme-mediated reactions. A notable example of such

organization is observed in the synthesis of highly branched and complex oligosaccharides in the Golgi apparatus, where an ordered array of membrane proteins sequentially adds or removes glycans on a protein substrate. In this way, an exponential number of glycoforms can be produced simply by rearranging the order of modification as the substrate moves between the *cis* and *trans* cisternae.<sup>[1,2]</sup> This spatiotemporal, modular design can produce a variety of metabolically useful compounds from a small subset of enzymes without diverting resources toward producing, or possibly evolving, a new enzyme for catalyzing each desired reaction product. The strategies that cells use to organize metabolic and signaling cascades have inspired efforts in the laboratory to develop compartmentalized

and spatiotemporally controlled systems capable of performing multistep enzyme cascades.<sup>[3–5]</sup>


Compartmentalization provides many advantages over traditional batch processes because multiple reaction steps can be individually interrogated and optimized.<sup>[6]</sup> Recent work has demonstrated strategies to sequentially organize two or more enzymes on solid supports for performing multistep transformations.<sup>[5]</sup> For example, packed-bed reactors have been used to arrange enzymes in series using streptavidin, Ni-NTA, and anti-FLAG-coated beads.<sup>[7–10]</sup> Microfluidic devices integrated with valves or magnetic components have organized enzyme-coated beads in well-defined regions on a chip,<sup>[10–12]</sup> which was beneficial for reducing dead volume.<sup>[11]</sup> An important feature of multienzyme cascade systems is the ability to precisely control the order of each reaction. To demonstrate the importance of maintaining correct enzyme order in a reaction sequence, one study observed a  $\approx 200$ -fold increase in product yield when two enzymes were correctly ordered along a fluidic stream.<sup>[13]</sup> Of particular interest are methods that use site-selective immobilization to colocalize multiple enzymes on the same chip for circumventing the need to separate each reaction in different compartments, as demonstrated by Niemeyer and co-workers using DNA hybridization.<sup>[14]</sup> These examples illustrate the immense value in spatially organizing enzymes for increasing the yields of products in tandem reactions; however, this important work did not investigate how microfluidic chips with identical compositions can provide different mixtures of reaction products dependent on the order of modification.

In the present work, we describe a microfluidic reactor having two enzymes organized such that a substrate in the flow stream will encounter the enzymes sequentially. The two enzymes, peptidylarginine deiminase type 1 (PAD) and

J. Grant, Prof. M. Mrksich  
Department of Chemistry  
Northwestern University  
Evanston, IL 60208, USA  
E-mail: milan.mrksich@northwestern.edu

Dr. J. A. Modica, Prof. M. Mrksich, J. Roll  
Department of Biomedical Engineering  
Northwestern University  
Evanston, IL 60208, USA

P. Perkovich  
Department of Chemical & Biological Engineering  
Northwestern University  
Evanston, IL 60208, USA

 The ORCID identification number(s) for the author(s) of this article can be found under <https://doi.org/10.1002/smll.201800923>.

DOI: 10.1002/smll.201800923

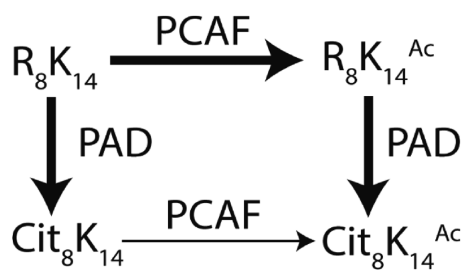


**Figure 1.** Schematic of crosstalk between Arg8 citrullination and Lys14 acetylation on the H3 peptide substrate. PCAF modifies K<sub>14</sub> at a high rate if R<sub>8</sub> is uncitrullinated. However, PCAF modifies K<sub>14</sub> at a much slower rate if R<sub>8</sub> is citrullinated.

acetyltransferase p300/CBP associated factor (PCAF) catalyze citrullination and acetylation, respectively, on a histone H3-derived peptide substrate (Ac-TARK<sup>Ac</sup>STGGKAPC). These two enzymes were of particular interest because treatment of the substrate with the two enzymes gives different products depending on the enzyme order.<sup>[15]</sup> This temporal dependence is due to a “crosstalk” wherein PCAF is unable to acetylate a peptide that is first citrullinated, though the acetylation state has no effect on PAD-mediated citrullination of the peptide (Figure 1). By spatially organizing PAD and PCAF along the fluidic chip we can tailor the device in favor of citrullinated or acetylated H3 peptide production.

## 2. Results

### 2.1. Design of the Spatiotemporal Fluidic System

Our approach is based on a microfluidic chip that has one enzyme covalently patterned on the chip surface for a defined length and the second enzyme patterned in a downstream region of the channel for a defined length (Figure 2). In this way, a substrate introduced into the device will initially encounter the first enzyme which converts it to an intermediate—where the time for this first reaction depends on the flow rate and length of channel having the immobilized enzyme—

and which then encounters the second enzyme that converts the intermediate to the final product. Finally, the surface of the chip downstream of the second enzyme presents a thiol-reactive maleimide group that serves to capture the cysteine-containing substrate and products. Self-assembled monolayers for matrix-assisted laser desorption/ionization mass spectrometry (SAMDI-MS) offers the significant advantage of detecting and quantifying all reaction species—substrate, intermediate, and product—directly on the reactor chip. This ability to quantitate all reaction products on the chip avoids the need to isolate and analyze each product.

The chip is a glass slide modified with a self-assembled monolayer of alkanethiolates on gold presenting maleimide groups at a density of 5% against a tri(ethylene glycol) background. The latter prevents both nonspecific protein adsorption and immobilized protein denaturation,<sup>[16,17]</sup> and is important for ensuring a consistent enzyme density and maintaining the activity of the enzymes. We previously reported a protein immobilization method wherein fusion proteins are covalently attached to a self-assembled monolayer using chemically orthogonal irreversible ligands.<sup>[18,19]</sup> For this work we immobilized PAD and PCAF to different regions in the channel using two enzyme–substrate pairs (Figure 3). The first enzyme is SnapTag, an engineered O6-alkylguanine alkyltransferase that site-specifically reacts with benzylguanine and benzylchloropyrimidine derivatives via a nucleophilic cysteine.<sup>[20–22]</sup> The second enzyme is HaloTag, an engineered haloalkane dehalogenase that covalently reacts with primary alkylchlorides via a nucleophilic aspartate.<sup>[23]</sup> The HaloTag and SnapTag proteins react with capture ligands based on an alkyl chloride and benzylchloropyrimidine derivative, respectively, on the monolayer. We prepared the capture ligands with a free thiol to allow their immobilization to monolayers presenting the maleimide groups (Figure S1, Supporting Information).

We generated the HaloTag fusion protein from an expression construct based on the commercially available pET-16b vector, where HaloTag is N-terminally fused to PAD with an (EAAAK)<sub>4</sub> peptide linker. Similarly, we generated the SnapTag fusion protein as an N-terminal fusion to PCAF, separated by the standard (EAAAK)<sub>4</sub> helical linker. Hence, these fusion proteins—HaloTag-PAD (Halo-PAD) and SnapTag-PCAF (Snap-PCAF)—each have

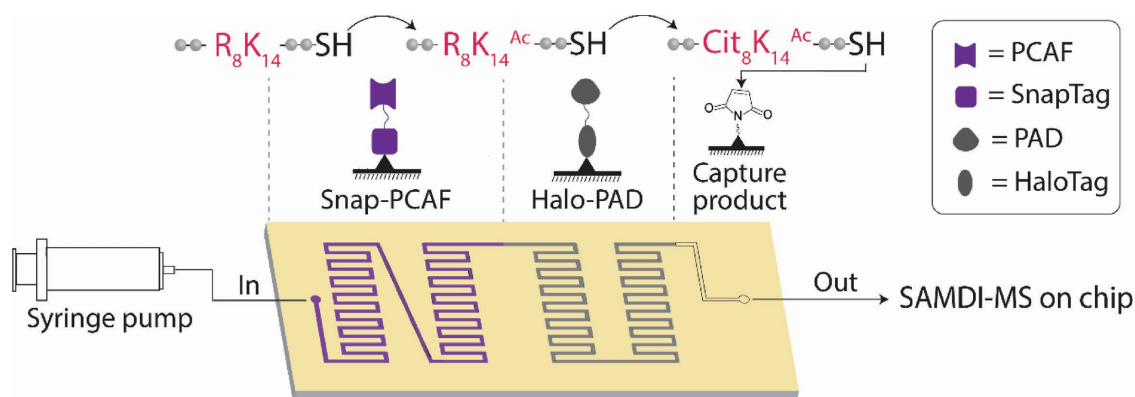


**Figure 2.** Overview of the reactor chip assembly and operation. A unidirectional microfluidic channel with an inlet and an outlet is placed onto a gold-coated microscope slide functionalized with a self-assembled monolayer. The chip has two enzymes, Snap-PCAF and Halo-PAD, patterned in discrete regions along the fluidic channel. A H3 peptide substrate flows through the chip—where it first encounters Snap-PCAF—and becomes acetylated. The acetylated product of the first reaction is the substrate for the next enzyme reaction by Halo-PAD, which citrullinates the peptide. A thiol on one end of the peptide covalently binds to maleimide functional groups in a downstream capture region. The products are analyzed by SAMDI-MS.

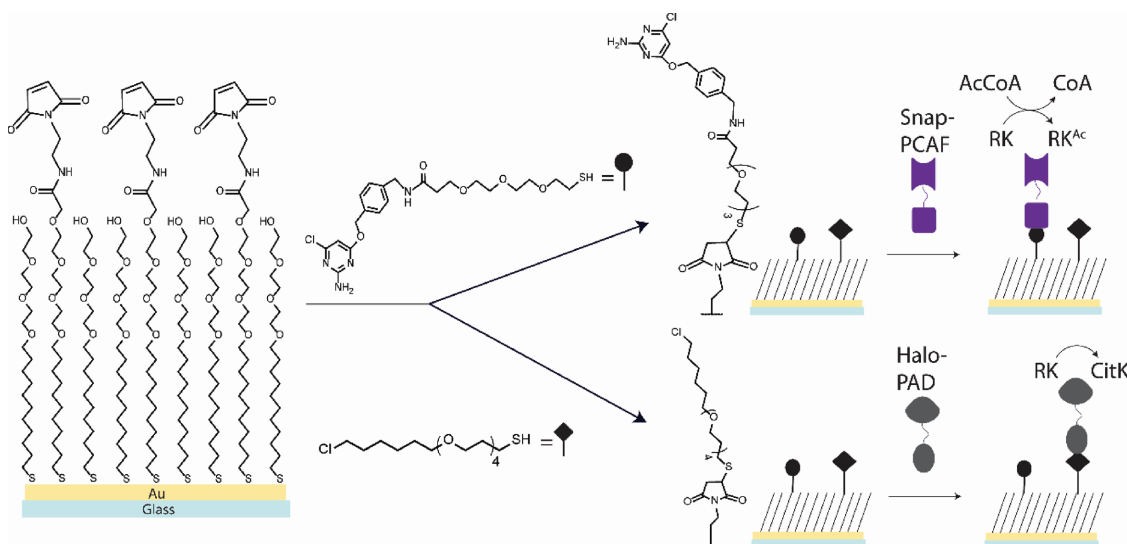


**Figure 3.** Strategy for PCAF and PAD immobilization. A self-assembled monolayer displaying maleimide is functionalized with SnapTag capture ligand (top) or HaloTag capture ligand (bottom) through reaction of the thiol. PCAF and PAD were prepared as SnapTag and HaloTag fusion proteins, respectively. The SnapTag domain is covalently captured via a benzylchloropyrimidine substrate and the HaloTag domain is captured via a hexylchloride to present PAD and PCAF on the surface of the self-assembled monolayer.

the enzyme domain that will be active in the channel and a capture domain that is used to immobilize them on the chip. We expressed the Halo-PAD construct in the BL21(DE3)pLysS *E. coli* strain and the Snap-PCAF construct in the BL21(DE3) *E. coli* strain. We expressed both fusion constructs using standard induction with isopropyl  $\beta$ -D-1-thiogalactopyranoside (IPTG) and purified expressed proteins using an included His-tag for nickel column affinity chromatography, followed by size exclusion chromatography. The resulting Halo-PAD and Snap-PCAF fusion proteins are 112.1 and 43.7 kDa, respectively (Figure S2, Supporting Information).

We fabricated the microfluidic element—which is subsequently brought into contact with the self-assembled monolayer—from polydimethylsiloxane (PDMS). We used 3D-printed molds instead of commonly used photolithographically patterned masters because 3D printing allowed us to rapidly prototype different designs without requiring use of a cleanroom and the ability to build and test many mold replicates in a short period of time (Figure S3, Supporting Information). 3D-printed molds have been previously fabricated using PDMS for microfluidic applications and post-treatment methods using combinations of heat, oxygen plasma, or silanization have been reported to improve PDMS polymerization on the 3D-printed mold.<sup>[24,25]</sup> Here, we simply heat-treated PolyJet 3D-printed molds and then poured the PDMS prepolymer mixture directly into the mold. Our molds were printed using a Stratasys Connex 350 3D printer with VeroWhite material and the molds did not require any modification other than a simple heat treatment step to support PDMS polymerization and rapid removal.

## 2.2. Single Enzyme Reactions with Immobilized PCAF

We first investigated each of the enzyme-mediated reactions on its own, beginning with acetylation of the H3 peptide in a chip

having immobilized Snap-PCAF followed by a downstream region presenting the maleimide group for effluent capture (Figure S4a, Supporting Information). We first patterned the SnapTag capture ligand on a stripe of the monolayer by reacting the ligand on the maleimide monolayer for 1 h. **Figure 4** shows a schematic of the procedure for operating the device once the capture ligand has been patterned. We aligned the PDMS block (derived from the master in Figure S3a, Supporting Information) with microchannel features onto the self-assembled monolayer, ensuring that the SnapTag capture ligand was located upstream of the effluent capture region. We inserted tubing into the inlet and outlet with the inlet connected to a pressure-driven syringe pump. We primed the device with Tris HCl (pH 8.5) buffer containing Triton X-100, then injected a solution of Tris HCl (pH 8.5) buffer containing Snap-PCAF and Triton X-100 to immobilize the enzyme. The Triton X-100 was added to further ensure nonspecific protein adsorption to the chip and channel walls. We next washed any remaining Snap-PCAF out of the device using Tris HCl (pH 8.0) buffer. Finally, we removed the outlet tubing, dried the tubing with nitrogen, and inserted it back into the device.

To verify the acetyltransferase activity of Snap-PCAF, we flowed the H3 peptide substrate at a flow rate ranging between 0.1 and 0.4  $\mu\text{L min}^{-1}$ . After flowing for 1.5 reactor volumes, we collected the effluent (for subsequent analysis) and the PDMS slab was peeled off of the chip. The chip presenting the self-assembled monolayer was rinsed with ethanol and water and treated with 2,4,6-tri-hydroxyacetophenone (THAP) matrix in acetone to be subsequently analyzed by SAMDI-MS. We noticed that the matrix crystallized more densely on the region of the reactor chip exposed to the channel, which enabled us to easily locate the captured reaction species using the video camera in the matrix-assisted laser desorption/ionization mass spectrometry (MALDI-MS) instrument.

Performing SAMDI-MS on the reactor chip produced spectra with mass-to-charge values corresponding to the H3 peptide bound to the maleimide-terminated alkanethiolate

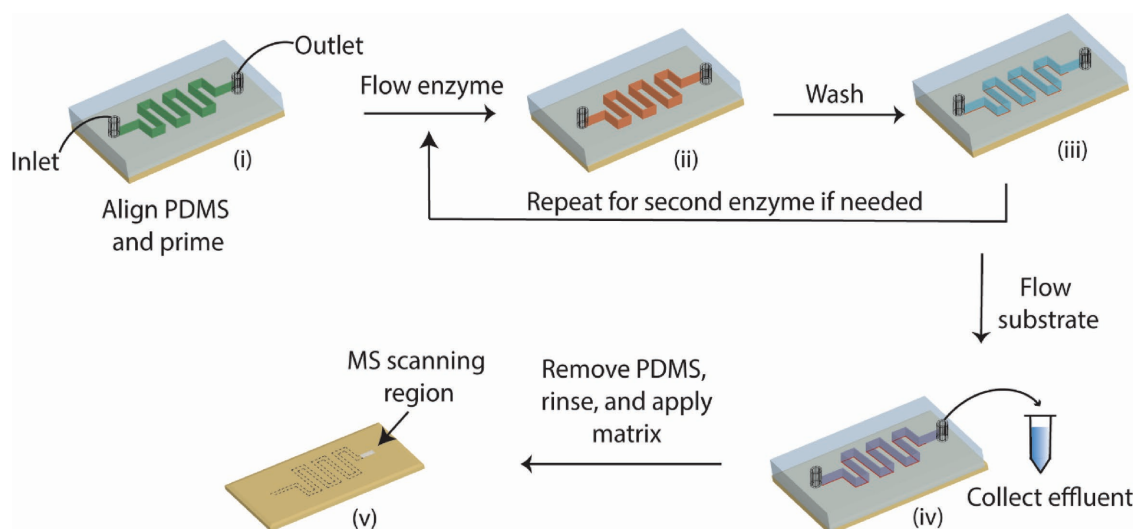


**Figure 4.** Procedure for fabricating and operating the fluidic reactor on the self-assembled monolayer. A PDMS block with microchannel features is placed on the chip prepared in Figure S4 (Supporting Information) with tubing inserted into the inlet and outlet. The outlet is located on the side of the chip that is free of capture ligand. i) The channel is primed with buffer and ii) the enzyme is flowed through the chip. iii) A wash step removes nonimmobilized enzyme and steps (ii) and (iii) are repeated if a second enzyme will be immobilized on the chip. iv) A solution of peptide substrate and cofactors are introduced at the inlet and the effluent is collected. v) The PDMS block is peeled from the chip and the effluent capture region is analyzed by SAMDI-MS.

(and the corresponding disulfide) (Figure 5a). Acetylation by PCAF corresponds to an increase in molecular weight of 42 Da. We studied the effect of flow rate on PCAF acetylation by assembling reactors where substrate was flowed at 0.1, 0.2, 0.3, and 0.4  $\mu\text{L min}^{-1}$  (Figure 5b). It is significant that the geometry of our channel—where the height is 250  $\mu\text{m}$ —together with these flow rates ensure efficient mixing of substrates throughout the channel. We calculated the product yield from Equation (1) using the integrated area under the peaks (AUP) for the substrate and product (Figure S5, Supporting Information)

$$\% \text{ product} = \frac{\text{AUP}_{\text{product}}}{\text{AUP}_{\text{product}} + \text{AUP}_{\text{substrate}}} \times 100 \quad (1)$$

These data reveal that PCAF acetylates  $\text{K}_{14}$  and that decreasing the substrate flow rate increases the yield of acetylated product. This result supports other immobilized enzyme systems that report an increase in product yield at decreasing flow rates—likely attributed to mass transfer effects.<sup>[26,27]</sup> Next, we ran a control experiment where we flowed a synthetically citrullinated H3 peptide  $\text{Cit}_8\text{K}_{14}$  at 0.1  $\mu\text{L min}^{-1}$  over immobilized Snap-PCAF to confirm that citrullination decreases the yield of acetylated peptide (Figure S6a, Supporting Information).

To determine the product yield from the collected effluent, we incubated the effluent for 1 h on a separate chip presenting a maleimide at a density of 10%. We repeated the SAMDI-MS analysis steps previously described for each flow rate. The product yield calculated on the reactor chip matched the product yield on the collected effluent chip, demonstrating that the reaction and analysis can both be carried out on the reactor chip. This saves time and material associated with collecting the effluent for subsequent analysis.

### 2.3. Single Enzyme Reactions with Immobilized PAD

We performed analogous experiments to confirm the citrullination of the peptide by PAD. Using a mass spectrometric readout was challenging because conversion of arginine to citrulline increases the substrate mass by only 1 Da. To address this problem, we chemically derivatized the citrulline moiety by reaction with phenylglyoxal prior to analysis with SAMDI-MS (Figure 6a). Phenylglyoxal has been previously shown to specifically react with the ureido group of citrulline residues using acidic conditions at elevated temperatures.<sup>[28]</sup> To initially demonstrate that this labeling strategy works well on our self-assembled monolayers presenting the H3 peptide, we immobilized the H3 peptide containing residues  $\text{R}_8\text{K}_{14}^{\text{Ac}}$  and  $\text{Cit}_8\text{K}_{14}^{\text{Ac}}$  on separate monolayers. We applied a solution of phenylglyoxal in 30% trifluoroacetic acid in water at 45 °C for 45 min. We observed complete conversion of the  $\text{Cit}_8\text{K}_{14}^{\text{Ac}}$  peptide to the expected phenylglyoxal adduct, as indicated by a +116 Da mass increase. None of the uncitrullinated  $\text{R}_8\text{K}_{14}^{\text{Ac}}$  peptide was converted to the phenylglyoxal adduct, demonstrating that this method is selective for citrulline. We also showed that this method is quantitative by immobilizing known ratios of  $\text{R}_8\text{K}_{14}^{\text{Ac}}$  and  $\text{Cit}_8\text{K}_{14}^{\text{Ac}}$  peptide and determining the percent of “product” information from the SAMDI spectra (Figure S7, Supporting Information). Phenylglyoxal selectively modified the citrulline moiety in a mixture of arginine and citrulline-containing peptides. This experiment also demonstrates that the two peptides bind to the self-assembled monolayer at approximately the same rate.

Using the same assay described for Snap-PCAF, we confirmed deiminase activity of immobilized Halo-PAD. After treating the reactor chip and collected effluent chip with phenylglyoxal, the SAMDI-MS spectra revealed a +116 mass shift indicative of the H3 peptide with phenylglyoxal-modified

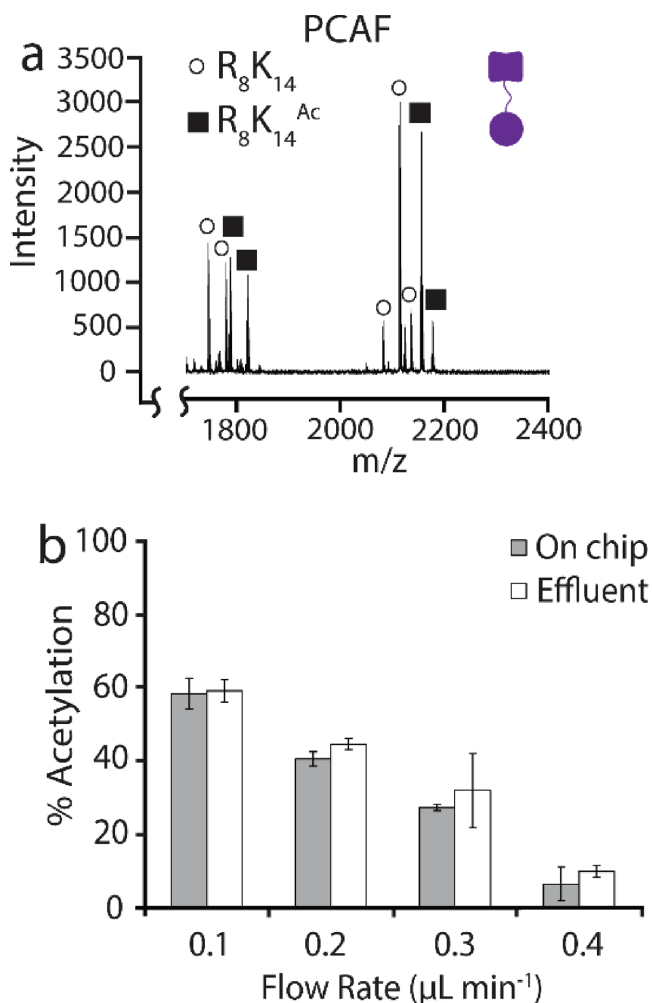


**Figure 5.** a) A SAMDI-MS spectrum of the collected effluent from the PCAF reactor. Acetylation increases the substrate mass by 42 Da. The proton, sodium, and potassium monoisotopic substrate (circles) and product peaks (squares) were integrated to calculate the percent of acetylated product. b) The yield of the acetylated product was calculated from the reactor chip and collected effluent at different flow rates. Mean  $\pm$  SD ( $n = 3$ ).

citrulline. Next, we studied the effect of flow rate on PAD citrullination by preparing separate reactors for each flow rate experiment (Figure 6c). Similar to PCAF, the yield of citrullinated product increases when flow rate decreases. However, conversion by PAD appears to be more sensitive to changes in flow rate than does PCAF. We also made a synthetically acetylated H3 peptide (R<sub>8</sub>K<sub>14</sub><sup>Ac</sup>) and determined immobilized Halo-PAD activity at 0.1  $\mu\text{L min}^{-1}$  using the methodology described above to confirm that PCAF acetylation does not affect Halo-PAD activity (Figure S6b, Supporting Information).

#### 2.4. Spatiotemporally Controlled Tandem Enzyme Reactions

PCAF and PAD participate in a “crosstalk” where they act on a peptide derived from histone H3. Initial citrullination of R<sub>8</sub> strongly decreases the acetylation of residue K<sub>14</sub> by PCAF. Hence, the three products that follow from treatment

of the peptide by the two enzymes—R<sub>8</sub>K<sub>14</sub><sup>Ac</sup>, Cit<sub>8</sub>K<sub>14</sub>, and Cit<sub>8</sub>K<sub>14</sub><sup>Ac</sup>—are formed in different yields depending on the order of enzyme treatment. We controlled the order of the two reactions by sequentially patterning PCAF and PAD along the reactor chip. Using the “NU” PDMS block as a reference (derived from the master in Figure S3b, Supporting Information) we prepared two reactor chips labeled pattern I and pattern II. Pattern I was generated by binding the SnapTag ligand for PCAF capture on the upstream “N” and the HaloTag ligand for PAD capture on the downstream “U” region. Pattern II was generated by binding the HaloTag ligand for PAD capture on the upstream “N” and the SnapTag ligand for PCAF capture on the downstream “U” region (Figure 7a,b). To immobilize each enzyme, we flowed Halo-PAD, buffer, and then Snap-PCAF through the channel. We then flowed the substrate ( $100 \times 10^{-6}$  M) at 0.1  $\mu\text{L min}^{-1}$  and analyzed the products that were captured to the monolayer as described earlier. The flow rate of 0.1  $\mu\text{L min}^{-1}$  was chosen because it resulted in the highest acetylated and citrullinated product yield within a reasonable operating time of 3.5 h. SAMDI-MS spectra reveal peaks with a +116 and +158 Da mass shift, representing the Cit<sub>8</sub>K<sub>14</sub> and Cit<sub>8</sub>K<sub>14</sub><sup>Ac</sup> products, respectively, in both patterns (Figure 7c,d, and Figure S8, Supporting Information). Mass spectra from pattern I show that Cit<sub>8</sub>K<sub>14</sub><sup>Ac</sup> and Cit<sub>8</sub>K<sub>14</sub> are the major products that comprise  $\approx 90\%$  of the product fraction. Strikingly, the spectra from pattern II reveal only one major product, Cit<sub>8</sub>K<sub>14</sub>, that comprises  $\approx 70\%$  of the product fraction. The remainder of the product fraction in pattern II consists of small quantities of R<sub>8</sub>K<sub>14</sub>, R<sub>8</sub>K<sub>14</sub><sup>Ac</sup>, and Cit<sub>8</sub>K<sub>14</sub><sup>Ac</sup>. The differences in product composition from patterns I and II reveal a strong dependence on enzyme order in the production of Cit<sub>8</sub>K<sub>14</sub> and Cit<sub>8</sub>K<sub>14</sub><sup>Ac</sup>. Additionally, we ran a set of control studies where we individually immobilized Snap-PCAF or Halo-PAD on the “N” or the “U” to confirm that patterning Halo-PAD upstream of Snap-PCAF contributes to the reduction in acetylated product (Figure S9, Supporting Information). Taken together, spatiotemporally organizing both enzymes on the chip gave distinct products that were consistent with the PAD-dependent crosstalk. Additionally, the product yield on the reactor chip approximates the product yield from the effluent in both patterns. This feature adds great utility to the reactor as the analysis is performed directly on the chip.

### 3. Discussion

In this paper, we describe a spatiotemporal approach for organizing enzymes and substrates that participate in a multistep reaction. We use a microfluidic device paired with self-assembled monolayers to enable enzymes to be sequentially patterned along the chip surface. In this way, a substrate introduced into a flowing buffer encounters the enzymes separately and in an order dictated by the direction of flow. Because we used two enzymes that install post-translational modifications on a peptide substrate—and where there is a “crosstalk” between the enzymes—we demonstrated that the major product depended on the order of enzyme treatment. This principle, where the spatiotemporal organization of a common set of reactants can

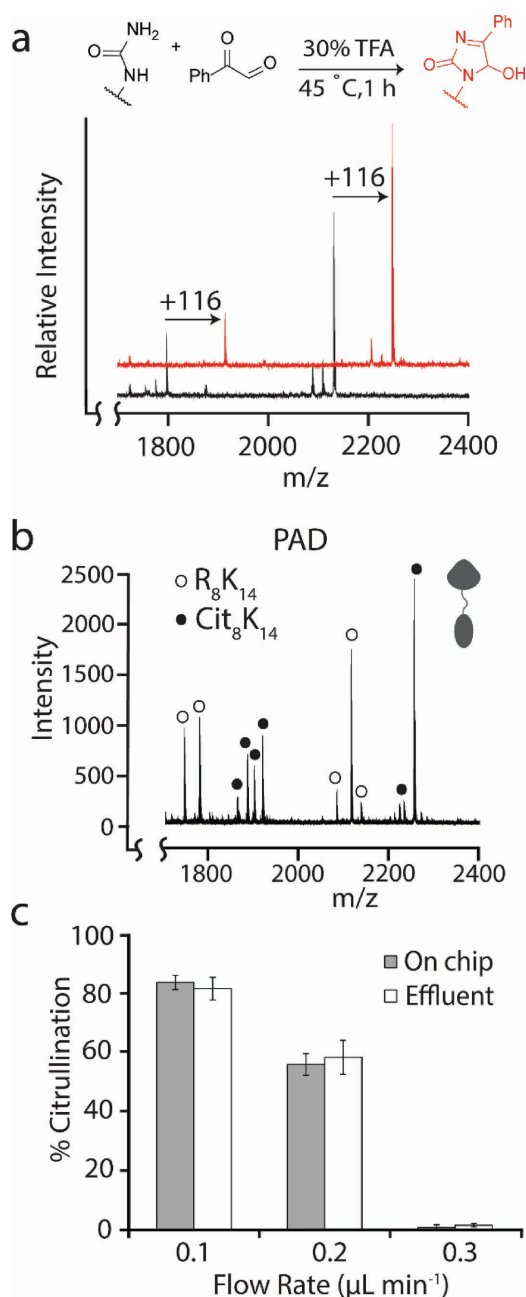


**Figure 6.** a) SAMDI-MS spectra of unconverted substrate (black,  $R_8K_{14}^{Ac}$ ) after treatment with phenylglyoxal show no mass shift. Treating citrullinated substrate (red,  $\text{Cit}_8K_{14}^{Ac}$ ) with phenylglyoxal is quantitative and increases the mass by 116 Da. b) SAMDI-MS spectrum of the collected effluent labeled with phenylglyoxal from the PAD reactor. The proton, sodium, and potassium monoisotopic substrate peaks (open circles) and product peaks (closed circles) were integrated to calculate the percent of citrullinated product. c) The citrullinated product yield was calculated at different flow rates from the collected effluent and on the reactor chip. Mean  $\pm$  SD ( $n = 3$ ).

give different reaction products, is a common feature in biology but remains little explored in traditional organic synthesis.<sup>[29]</sup>

The device benefits from a modularity which allowed us to study a reaction sequence step-by-step and analyze the products on the same chip. The ability to independently vary the position

of each enzyme and the reaction time of the substrate over the immobilized enzymes gave distinct product mixtures. In addition, the ability to perform a multistep enzyme reaction and quantify the reaction products directly on the fluidic chip simplified analysis while negating the need to sacrifice effluent for downstream product analysis. This single-surface approach to reactivity and detection should be broadly applicable to other multienzyme reaction systems.

It is significant that the product yields from the collected effluent approximately equal the yield observed on the reactor chip. The lateral channel length required for complete mixing in the axial ( $z$ -direction) at 0.1, 0.2, 0.3, and 0.4  $\mu\text{L min}^{-1}$  flow rates was 61.7, 123.4, 185.1, and 246.84  $\mu\text{m}$ , respectively ( $D = 4.22 \times 10^{-6} \text{ cm}^2 \text{ s}^{-1}$ <sup>[30]</sup>,<sup>[31]</sup>). The diffusion lengths were very small compared to the length of the microfluidic channels ( $\approx 181.2 \text{ mm N}$ ,  $\approx 181.2 \text{ mm U}$ ,  $\approx 12.5 \text{ mm maleimide capture region}$ ), thus the exchange between the reaction products and bulk occurred rapidly and did not generate large concentration gradients throughout the length of the device. We also referred to work by Manalis and co-workers to consider the possible generation of a thin depletion layer of peptide directly above the immobilized enzyme and maleimide capture regions.<sup>[32]</sup> That work reported COMSOL simulations of biosensors with analyte flowing into a rectangular channel and becoming captured in a downstream region. We found that a depletion zone does not exist over the immobilized enzyme (“N” or “U”), and a very thin depletion zone relative to the height of the channel exists over the maleimide capture region. We expect that this thin depletion zone lowered the concentration of analyte directly above the maleimide capture region. We observe complete binding of analyte to the maleimide throughout the capture region, confirming that the depletion zone does not lower the concentration of the analyte enough to prevent complete reaction with the surface.

Patterning two enzymes on a microfluidic chip facilitated the conversion of the substrate first to an intermediate, and finally to the product. Three recent reports also describe the patterning of two enzymes on a solid support and observed enhanced rates of product formation through substrate channeling.<sup>[33–35]</sup> Those examples did not use flow to deliver the intermediate to the second enzyme but instead relied on diffusion. Our example ensures a more efficient transfer of the intermediate to the second enzyme. Further, microfluidic devices have a large surface-to-volume ratio and small length scales that allow for fast mass transfer, which can serve to remove inhibitory products and reduce product inhibition of the enzymes.<sup>[6]</sup>

The use of self-assembled monolayers enabled important features of our approach. Taking advantage of the ability to control the surface chemistry, we were able to use enzyme-reactant pairs to covalently functionalize the surface with enzymes of interest. A tri(ethylene glycol) background provided resistance to nonspecific adsorption, giving the necessary control needed to pattern proteins. Additionally, the self-assembled monolayers provided an elegant way of capturing and analyzing the resulting products of the enzyme reactions directly on the chip. The reaction products were flowed over and captured on regions of monolayer functionalized with maleimide, allowing the products to be analyzed directly by SAMDI-MS. SAMDI-MS has been applied to measuring a broad range of enzyme

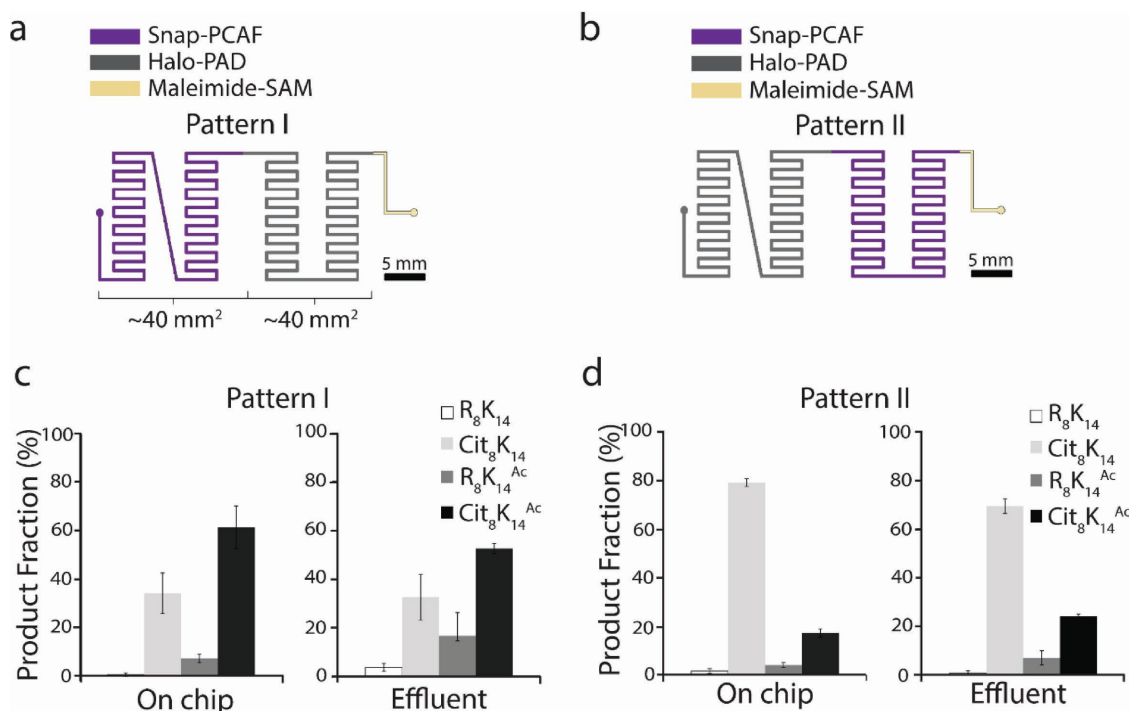


**Figure 7.** a) Regions of the fluidic channel with Snap-PCAF (purple), Halo-PAD (gray), and available for effluent capture (gold). The fluidic channel has a “NU” design, where each enzyme is patterned on either the “N” or the “U” and the “N” and “U” each have a surface area of 40 mm<sup>2</sup>. Pattern I has Snap-PCAF patterned on the “N” and Halo-PAD patterned on the “U.” b) Quantitation of R<sub>8</sub>K<sub>14</sub>, R<sub>8</sub>K<sub>14</sub><sup>Ac</sup>, Cit<sub>8</sub>K<sub>14</sub>, and Cit<sub>8</sub>K<sub>14</sub><sup>Ac</sup> yields on the reactor chip and from the collected effluent in pattern I. Mean ± SD (n = 3). c) Pattern II has Halo-PAD patterned on the “N” and Snap-PCAF patterned on the “U.” d) Quantitation of R<sub>8</sub>K<sub>14</sub>, R<sub>8</sub>K<sub>14</sub><sup>Ac</sup>, Cit<sub>8</sub>K<sub>14</sub>, and Cit<sub>8</sub>K<sub>14</sub><sup>Ac</sup> yields on the reactor chip and from the collected effluent in pattern II. A reduction in Cit<sub>8</sub>K<sub>14</sub><sup>Ac</sup> and increase in Cit<sub>8</sub>K<sub>14</sub> is observed in pattern II, where PAD precedes PCAF in the reaction sequence. Mean ± SD (n = 3).

activities and offers a general method for quantitating reaction products.<sup>[36a–e]</sup>

We were able to covalently and selectively pattern enzymes in defined regions on the 2D reactor surface by using orthogonal active site chemistries for immobilization. This allowed us to know exactly where each reaction took place and to control the reaction times of substrate and intermediates over the immobilized enzymes. DNA hybridization has also been used to pattern areas of active enzyme on a variety of DNA architectures in microfluidic and nonmicrofluidic systems.<sup>[33,34,37–42]</sup> This method has been applied toward studying single enzyme activities and multienzyme reaction cascades. Our approach uses covalently bound enzymes that generate a permanent bond between the enzyme and the surface. Expressing the handle for protein immobilization as a fusion protein is advantageous because it does not require chemical modification of the enzymes after expression—a process which can reduce enzyme activity and yield.

We also showed that phenylglyoxal can be used to selectively modify citrullinated products for detection by mass spectrometry. This method has wide applications beyond the system reported in this paper, as recent work has suggested that the PAD family of enzymes play pathophysiological roles in a variety of human diseases including rheumatoid arthritis, psoriasis, cancer, Alzheimer’s disease, and multiple sclerosis.<sup>[43]</sup> Compounds that inhibit certain PAD isoforms show promise in treating or slowing down the progression

of these diseases.<sup>[44,45]</sup> Profiling the substrate specificity of PAD isoforms will generate insight for developing selective inhibitors.<sup>[46]</sup> Previous assays have used trypsin to detect citrullination with mass spectrometry because it cleaves after arginine residues but not citrulline residues.<sup>[47]</sup> However, trypsin also cleaves lysine residues, which complicates the analysis of substrates containing a mixture of trypsin cleavage sites. Phenylglyoxal labeling is a direct and quantitative method for identifying the substrate specificity of PAD isoforms on different peptide sequences.<sup>[48]</sup> We were able to quantitatively label Cit<sub>8</sub>K<sub>14</sub><sup>Ac</sup> and Cit<sub>8</sub>K<sub>14</sub> with phenylglyoxal to address the extent of citrullinated product yield on the reactor chip.

We also describe a method to cast PDMS directly onto 3D-printed molds, overcoming the time and facility barriers constraining current photolithographic methods to prepare PDMS molds. 3D printing enabled us to rapidly prototype different mold designs and build many mold replicates in less time without the need for specialized facilities. We describe a method that only requires a heat treatment step after 3D printing to allow PDMS polymerization and rapid removal. This method can be applied to a wide variety of channel designs as well as in applications outside of microfluidics such as single cell analysis, nanoparticle synthesis, and soft robotics.<sup>[49–51]</sup> Future work may use 3D printing to create the entire microfluidic device, as described by Folch and co-workers.<sup>[52,53]</sup>

## 4. Conclusion

The approach we describe here may be extended to other enzyme-mediated transformations for targeted biosynthesis of products and mixtures. Advantages over existing procedures that use packed-bed capillaries or planar supports are that reaction product depends on the order of enzyme covalently immobilized to the channel floor and that product analysis occurs on the chip.<sup>[7,11]</sup> Tuning the flow rate and order of patterned enzymes allows for the step-by-step optimization of complex biosynthetic pathways. Systems that rigorously separate and control the order of enzyme reactions can be used for accessing specific biosynthetic products in high yields. We believe this approach is simpler and more versatile than many other methods for carrying out and studying multistep enzyme reactions, and it will find many applications in biochemical syntheses.

## 5. Experimental Section

**Reagents:** THAP, acetyl coenzyme A, phenylglyoxal hydrate,  $\beta$ -D-thioglyucose sodium salt, and complete protease inhibitor tablets (EDTA-free) were purchased from Sigma Aldrich. Amino acids and peptide synthesis reagents were purchased from Anaspec. pET-16b vectors encoding for Snap-PCAF and PAD1 were obtained from Thermo Fisher Scientific—GeneArt with the codons optimized for *E. coli* expression. Oligonucleotide primers were purchased from Integrated DNA Technologies. Bug Buster (10 $\times$ ) was purchased from EMD Millipore. BL21DE3 *E. coli* and Gibson Assembly Master Mix were purchased from New England Biolabs. BL21DE3pLysS *E. coli* was purchased from Promega. PDMS prepolymer mixture was purchased from Ellsworth Adhesives. Neodymium magnets were purchased from Ace Hardware and Amazon.com. The H3 peptide (Ac-TARK<sup>Ac</sup>STGGKAPC), acetylated H3 peptide (Ac-TARK<sup>Ac</sup>STGGK<sup>Ac</sup>APC), and citrullinated H3 peptide (Ac-TACitK<sup>Ac</sup>STGGK<sup>Ac</sup>APC) were prepared using standard Fmoc solid-phase peptide synthesis methods on Rink Amide MBHA resin.<sup>[54]</sup>

**Assembly of Halo-PAD Construct:** Halo-PAD was assembled using standard Gibson assembly protocols (New England Biolabs) using polymerase chain reaction (PCR) from a vector containing HaloTag and a vector containing (EAAAK)<sub>4</sub>-PAD. The primers used to PCR the vector containing HaloTag are: 5'-CCATATCGAAGGTCGTCATATGGAAATCGGTA CTGGCTTCC-3' (forward) and 5'-GCTGCTCTCCAATTGAATCTCCAGAGTAGACAGCC-3' (reverse). The primers to PCR the vector containing (EAAAK)<sub>4</sub>-PAD are: 5'-GGCTGTCTACTCTGGAGATTCAATTGGAAGCAGCAGC-3' (forward) and 5'-GGAAGCCAGTACCGATTCCATATGACGACCTTCGATATGG-3' (reverse).

**Protein Expression and Purification:** To express Snap-PCAF, the vector was transformed into BL21DE3 *E. coli* using chemical transformation methods. A stab of Snap-PCAF BL21DE3 was added to 2xYT media (5 mL) with carbenicillin and allowed to grow overnight at 30 °C while shaking at 240 rpm. The next morning, the culture was added to 2xYT media (500 mL) supplemented with carbenicillin (100  $\mu$ g mL<sup>-1</sup>) and grown at 30 °C while shaking until the OD<sub>600</sub> reached  $\approx$ 0.45. The culture was cooled at 4 °C and Snap-PCAF expression was induced with 0.5  $\times$  10<sup>-3</sup> M IPTG overnight under shaking at 16 °C. The bacteria were pelleted by centrifugation and lysed in buffer (50  $\times$  10<sup>-3</sup> M Tris pH 8.5, 200  $\times$  10<sup>-3</sup> M NaCl, 5  $\times$  10<sup>-3</sup> M  $\beta$ -mercaptoethanol, 50 mL) containing Bug Buster (10 $\times$ , 2 mL) and one cOmplete-Mini protease inhibitor tablet. The overexpressed Snap-PCAF contains a N'-terminal His tag and was purified on a nickel immobilized nickel affinity resin (IMAC) column. Fractions eluted off of the nickel column were combined and concentrated to 1 mL in a 25 mL Amicon 10 kDa cutoff Centrifugal Filter Unit (Millipore). The Snap-PCAF was further purified using size exclusion

chromatography on an Akta FPLC (GE Healthcare) using running buffer (50  $\times$  10<sup>-3</sup> M Tris pH 8.5, 200  $\times$  10<sup>-3</sup> M NaCl). Fractions containing Snap-PCAF were confirmed by sodium dodecyl sulfate polyacrylamide gel electrophoresis (SDS-PAGE), pooled and concentrated, and stored at -80 °C in 50% glycerol. To express Halo-PAD, the vector was transformed into BL21DE3pLysS *E. coli* using chemical transformation methods. A stab of Halo-PAD BL21DE3 was added to 2xYT media (5 mL) with carbenicillin and allowed to grow overnight at 30 °C while shaking. The culture was then added to 2xYT media (500 mL) supplemented with carbenicillin and grown at 30 °C with shaking until the OD<sub>600</sub> reached  $\approx$ 0.50. The culture was cooled at 4 °C and Halo-PAD expression was induced with IPTG (0.5  $\times$  10<sup>-3</sup> M) overnight under shaking at 25 °C. The bacteria were pelleted by centrifugation and lysed in buffer (50 mL) Tris pH 8.0 (50  $\times$  10<sup>-3</sup> M), NaCl (300  $\times$  10<sup>-3</sup> M), containing 10 $\times$  Bug Buster (2 mL) and one Complete-Mini protease inhibitor tablet. The overexpressed Halo-PAD also contained a N'-terminal His tag and was purified on a nickel resin column. Fractions eluted off of the nickel column were combined and concentrated to 1 mL in a 25 mL Amicon 50 kDa cutoff Centrifugal Filter Unit (Millipore). The Halo-PAD was further purified using size exclusion chromatography on an Akta FPLC (GE Healthcare) using running buffer Tris pH 8.0 (50  $\times$  10<sup>-3</sup> M) and NaCl (300  $\times$  10<sup>-3</sup> M). Fractions containing Halo-PAD were confirmed by SDS-PAGE, pooled and concentrated, and stored at -80 °C in 50% glycerol.

**3D Printing Molds:** The two mold designs in Figure S3 (Supporting Information) were rendered on SolidWorks software. The first consists of a single winding channel to test individual PCAF and PAD activity, while the second contains a single channel spelling out 'NU' to test both PCAF and PAD activities. The channel width and height was 250  $\mu$ m  $\times$  250  $\mu$ m, and the inlet and outlet diameters were 800  $\mu$ m for both designs. The files were converted to .stl format and printed in digital printing mode using a Stratasys Connex 350 3D printer in VeroWhite material (Stratasys Direct) with a glossy finish. The designs were organized on the build surface so that the printing striations lie parallel to the longest side of each part. The support material was placed on the bottom of the mold not contacting the channel features. We included 3 mm walls in our mold design because we found that PDMS will not polymerize on the side of the mold previously exposed to support material even after several 43 °C heat treatment cycles. After printing, the support material was removed with a WaterJet. The 3D-printed parts were washed with ultrapure water, dried over a nitrogen stream, and placed in a 43 °C oven for 48 h before using as PDMS molds. We noticed that the PDMS did not polymerize on the mold without this heat treatment.

**Self-Assembled Monolayer Preparation on Gold Surfaces:** Standard glass microscope slides were cleaned using ethanol and water in a sonication bath. An electron beam evaporator was used to deposit 5 nm Ti (0.02 nm s<sup>-1</sup>) followed by 30 nm Au (0.05 nm s<sup>-1</sup>). Two types of slides were prepared for each experiment: the microfluidic reactor slides and the effluent capture slides. The microfluidic reactor slides were soaked overnight at 25 °C in an ethanolic solution (0.5  $\times$  10<sup>-3</sup> M total disulfide concentration); the solution had a 1:9 of an asymmetric disulfide terminated with a maleimide group and a tri(ethylene glycol) group, and a symmetric disulfide terminated with tri(ethylene glycol) groups. Likewise, the effluent capture slides were soaked overnight under the same conditions except for the ratio of asymmetric:symmetric disulfide, which was changed to 1:4. The slides were then rinsed with ethanol and water. A glass etcher was used to create a marking 16.8 mm from the short edge of the Au slide, indicating the location of the outlet. For studies where only PCAF or PAD were bound to the slide, another marking was made 24.6 mm away from the same edge of the Au slide. This second marking indicated the boundary between the enzyme binding region and the product capture region. A rectangular piece of PDMS 3 mm in width and height was aligned to the right of the 24.6 mm marking, in between the 24.6 mm marking and 16.8 mm marking. Neodymium magnets were placed on the top of the PDMS piece and on the bottom of the slide, securing the PDMS onto the slide and establishing a physical boundary for the effluent capture region and enzyme immobilization region. A solution (200  $\mu$ L) containing either the HaloTag immobilization ligand (100  $\times$  10<sup>-6</sup> M) or SnapTag immobilization



ligand ( $100 \times 10^{-6} \text{ M}$ ) in a 1:3 ratio of Tris pH 8.0 ( $100 \times 10^{-3} \text{ M}$ ) and Triton X-100 (0.01%) was pipetted onto the enzyme binding region and incubated at  $25^\circ\text{C}$  for 1 h in a humidity chamber.  $\beta$ -D-thioglucoase was used to block the maleimide groups for the control experiments. The chips were rinsed with ethanol and water, and dried under a stream of  $\text{N}_2$ . For experiments involving PAD and PCAF to be present on the same chip, two additional markings were made in addition to the 16.8 mm marking; the first was made 23.01 mm away from the same edge of the Au slide, and the second was made 40.37 mm away from the same edge of the Au slide. A rectangular piece of PDMS was aligned to the right of the 40.37 mm marking and secured with neodymium magnets. A solution (200  $\mu\text{L}$ ) containing either the HaloTag immobilization ligand ( $100 \times 10^{-6} \text{ M}$ ), SnapTag immobilization ligand ( $100 \times 10^{-6} \text{ M}$ ), or  $\beta$ -D-thioglucoase ( $100 \times 10^{-6} \text{ M}$ ) in a 1:3 ratio of Tris pH 8.0 ( $100 \times 10^{-3} \text{ M}$ ) and Triton X-100 (0.01%) was pipetted onto the enzyme-binding region and incubated at  $25^\circ\text{C}$  for 1 h in a humidity chamber. Afterward, the chips were rinsed with ethanol and water, and dried under a stream of  $\text{N}_2$ . Next, the same process was repeated with the second immobilization ligand or  $\beta$ -D-thioglucoase using a piece of PDMS to block the 23.01 mm marking next to the effluent capture region. The chips were rinsed again with ethanol and water, and dried under a stream of nitrogen.

**Microfluidic Chip Fabrication:** PDMS prepolymer mixture was mixed in a 1:10 ratio (w/w curing agent to prepolymer), degassed in a vacuum desiccator for 15 min, and poured into a 3D-printed mold. The mold containing PDMS was degassed in a vacuum desiccator for 15 min and then placed in a  $43^\circ\text{C}$  oven overnight. The PDMS blocks were then peeled off of the mold and treated in a  $130^\circ\text{C}$  oven for 10 min. The 3D-printed molds were reused for additional PDMS-curing cycles. A 0.8 mm biopsy punch was used to generate inlet and outlet ports in the PDMS block. Once the self-assembled monolayer was prepared with the appropriate enzyme immobilization ligands, the PDMS block was treated with 50 W air plasma for 35 s at 200 mTorr using a Solarus Plasma Cleaner (Gatan, Inc.). The PDMS block was immediately aligned with the glass slide so that the outlet port was located over the effluent capture region 16.5 mm from the edge of the slide. The simple meandering channel design was used for chips only presenting one immobilization ligand while the "NU" design was used for chips presenting both capture ligands. The PDMS and Au chip assembly was then placed in a clamp made from extruded polycarbonate and secured by screws (Figure S10, Supporting Information). PTFE tubing was inserted into the outlet. Silicon tubing was placed in the inlet and connected to a syringe with  $\text{CaCl}_2$  ( $10 \times 10^{-3} \text{ M}$ ) and a 1:1 mixture of Tris pH 8.5 ( $100 \times 10^{-3} \text{ M}$ ), NaCl ( $50 \times 10^{-3} \text{ M}$ ), Triton X-100 (0.01%): PBS pH 7.4 (1 $\times$ ), Triton X-100 (0.01%). The chip was primed with this buffer using a syringe pump (Harvard Apparatus) at  $2.0 \mu\text{L min}^{-1}$  for 20 min. The buffer was freshly prepared before the start of each experiment and kept chilled at  $4^\circ\text{C}$  when not in use.

**Chip Operation for Individual Snap-PCAF and Halo-PAD Activities:** For chips only presenting the SnapTag immobilization ligand, a solution of Snap-PCAF ( $500 \times 10^{-9} \text{ M}$ ) was prepared in buffer with  $\text{CaCl}_2$  ( $10 \times 10^{-3} \text{ M}$ ) and a 1:1 mixture of Tris pH 8.5 ( $100 \times 10^{-3} \text{ M}$ ), NaCl ( $50 \times 10^{-3} \text{ M}$ ), Triton X-100 (0.01%): PBS pH 7.4 (1 $\times$ ), Triton X-100 (0.01%). The Snap-PCAF solution was injected into the microfluidic chip at  $1.0 \mu\text{L min}^{-1}$  for 35 min. Then, the inlet silicon tubing was replaced with PTFE tubing and buffer containing a  $\text{CaCl}_2$  ( $10 \times 10^{-3} \text{ M}$ ) and a 1:1 mixture of Tris pH 8.0 ( $100 \times 10^{-3} \text{ M}$ ), NaCl ( $50 \times 10^{-3} \text{ M}$ ): PBS pH 7.4 (1 $\times$ ), Triton X-100 (0.01%) was flowed for 5 min at  $5.0 \mu\text{L min}^{-1}$ . The outlet tubing was disconnected from the channel and dried with a stream of  $\text{N}_2$ . A buffer containing the H3 peptide ( $100 \times 10^{-6} \text{ M}$ ),  $\text{CaCl}_2$  ( $10 \times 10^{-3} \text{ M}$ ), and acetyl coenzyme A ( $100 \times 10^{-6} \text{ M}$ ) in 1:1 of Tris pH 8.0 ( $100 \times 10^{-3} \text{ M}$ ), NaCl ( $50 \times 10^{-3} \text{ M}$ ): PBS pH 7.4 (1 $\times$ ), Triton X-100 (0.01%) was flowed at 0.1, 0.2, 0.3, or  $0.4 \mu\text{L min}^{-1}$  for 1.5 reactor volumes. The clamp and PDMS assembly was disassembled from the Au reactor chip, washed with ethanol and water, and dried under  $\text{N}_2$ . The effluent in the outlet line was collected in a microcentrifuge tube. The collected effluent was reduced with TCEP ( $100 \times 10^{-6} \text{ M}$ ) for 10 min, and  $2.5 \mu\text{L}$  was spotted onto an effluent capture slide. The effluent was incubated on the slide for 1 h at  $25^\circ\text{C}$ , rinsed with ethanol and

water, and dried under  $\text{N}_2$ . The method for determining PAD activity was carried out using the same conditions stated above, except that a solution of Halo-PAD ( $200 \times 10^{-9} \text{ M}$ ) was flowed into the device and phenylglyoxal was used to modify the citrullinated product. To carry out the phenylglyoxal modification, a solution of phenylglyoxal hydrate (7.6 mg, 56.7 mmol) in trifluoroacetic acid and  $\text{H}_2\text{O}$  (30% trifluoroacetic acid, 70%  $\text{H}_2\text{O}$ , 0.5 mL) was freshly prepared. The solution (200  $\mu\text{L}$ ) was applied to the microfluidic reactor slide and the slide previously incubated with the collected effluent. The phenylglyoxal solution was incubated for 45 min at  $45^\circ\text{C}$ , rinsed with ethanol and water, and dried under  $\text{N}_2$ . A solution of THAP ( $25 \text{ mg mL}^{-1}$ ) in acetone (50  $\mu\text{L}$ ) was applied to each chip and the chips were analyzed using an AB Sciex 5800 MALDI TOF/TOF mass spectrometer. On the microfluidic reactor chip, spectra were obtained from the effluent collection region. Data Explorer software was used to measure the area under the monoisotopic peaks of the disulfides and thiolates (AB Sciex). This procedure was repeated for control studies with immobilized Snap-PCAF and Halo-PAD using the citrullinated H3 peptide (Ac-TACitK<sup>Ac</sup>STGGK<sup>Ac</sup>APC) and acetylated H3 peptide (Ac-TARK<sup>Ac</sup>STGGK<sup>Ac</sup>APC), respectively, at  $0.1 \mu\text{L min}^{-1}$ . All experimental conditions were repeated three times with three spectra obtained per experimental replicate.

**Chip Operation for Combined Snap-PCAF and Halo-PAD Activity:** After priming the chips presenting both immobilization ligands, a solution of Halo-PAD ( $200 \times 10^{-9} \text{ M}$ ) was prepared in a buffer with  $\text{CaCl}_2$  ( $10 \times 10^{-3} \text{ M}$ ) and a 1:1 mixture of Tris pH 8.5 ( $100 \times 10^{-3} \text{ M}$ ), NaCl ( $50 \times 10^{-3} \text{ M}$ ), Triton X-100 (0.01%): PBS pH 7.4 (1 $\times$ ), Triton X-100 (0.01%). The Halo-PAD solution was injected into the microfluidic chip at  $1.0 \mu\text{L min}^{-1}$  for 35 min. Then, the same buffer without containing Halo-PAD was injected at  $5.0 \mu\text{L min}^{-1}$  for 5 min. Next, a solution of Snap-PCAF ( $500 \times 10^{-9} \text{ M}$ ) was prepared in a buffer with  $\text{CaCl}_2$  ( $10 \times 10^{-3} \text{ M}$ ) and a 1:1 mixture of Tris pH 8.5 ( $100 \times 10^{-3} \text{ M}$ ), NaCl ( $50 \times 10^{-3} \text{ M}$ ), Triton X-100 (0.01%): PBS pH 7.4 (1 $\times$ ), Triton X-100 (0.01%). The outlet tubing was disconnected from the channel and dried with a stream of  $\text{N}_2$ . The H3 peptide ( $100 \times 10^{-6} \text{ M}$ ) in a buffer with  $\text{CaCl}_2$  ( $10 \times 10^{-3} \text{ M}$ ) and 1:1 Tris pH 8.0 ( $100 \times 10^{-3} \text{ M}$ ), NaCl ( $50 \times 10^{-3} \text{ M}$ ), and PBS pH 7.4 (1 $\times$ ) was flowed at  $0.1 \mu\text{L min}^{-1}$  for 1.5 reactor volumes. The remainder of the steps, including the phenylglyoxal modification step, were kept the same as previously described.

**Reactions to Generate a Phenylglyoxal Response Curve:** Standard glass microscope slides were cleaned using ethanol and water in a sonication bath. An electron beam evaporator was used to deposit 5 nm Ti ( $0.02 \text{ nm s}^{-1}$ ) followed by 30 nm Au ( $0.05 \text{ nm s}^{-1}$ ). The slides were soaked overnight at  $25^\circ\text{C}$  in an ethanolic solution ( $0.5 \times 10^{-3} \text{ M}$  total disulfide concentration); the solution had a 1:4 of an asymmetric disulfide terminated with a maleimide group and a tri(ethylene glycol) group, and a symmetric disulfide terminated with tri(ethylene glycol) groups. The slides were then rinsed with ethanol and water. Different solutions containing Ac-TARK<sup>Ac</sup>STGGK<sup>Ac</sup>APC and Ac-TACitK<sup>Ac</sup>STGGK<sup>Ac</sup>APC ( $100 \times 10^{-6} \text{ M}$ ) were prepared in Tris HCl 8.0 ( $100 \times 10^{-3} \text{ M}$ ), consisting of Ac-TARK<sup>Ac</sup>STGGK<sup>Ac</sup>APC, Ac-TACitK<sup>Ac</sup>STGGK<sup>Ac</sup>APC, and different ratios of each peptide to generate a linear calibration curve.  $2.5 \mu\text{L}$  of each peptide solution was individually spotted in separate areas of the slide to ensure that no mixing occurred and the slide was incubated in a humidity chamber for 1 h at  $25^\circ\text{C}$ . The slide was rinsed with ethanol and water, dried under a stream of  $\text{N}_2$ , and reacted with phenylglyoxal as previously described. The slide was treated with THAP matrix ( $25 \text{ mg mL}^{-1}$  in acetone) and three SAMDI-MS spectra were obtained from each spot. Adduct formation was quantified by calculating the integrated area under each monoisotopic peak as previously described. This experiment was repeated three times to generate the data obtained in Figure S7 (Supporting Information).

## Supporting Information

Supporting Information is available from the Wiley Online Library or from the author.

## Acknowledgements

This material is based upon work supported by the National Science Foundation Graduate Research Fellowship under Grant No. DGE-1324585. In addition, the project depicted was sponsored by the Department of the Defense, Defense Threat Reduction Agency HDTRA1-15-1-0052. This work used facilities of the Northwestern University 3D Printing and Rapid Prototyping Lab, the Northwestern University Integrated Molecular Structure Education and Research Center, the Northwestern University Structural Biology Core, the Northwestern University NUSeq Core, and the Northwestern University Research Shop—Instrumentation Design, Engineering, and Production. The authors thank Michael Wasukiewicz at the Northwestern University Research Shop—Instrumentation Design, Engineering, and Production for fabricating the device clamp. The authors also thank Alexander Simon for providing us with the vector encoding HaloTag. Any opinion, findings, and conclusions or recommendations expressed in this material are those of the authors(s) and do not necessarily reflect the views of the National Science Foundation. The content of the information does not necessarily reflect the position or the policy of the federal government, and no official endorsement should be inferred.

## Conflict of Interest

The authors declare no conflict of interest.

## Keywords

immobilized enzymes, MALDI mass spectrometry, microfluidics, microreactors, self-assembled monolayers

Received: March 8, 2018

Revised: June 7, 2018

Published online: July 3, 2018

- [1] T. R. Graham, S. D. Emr, *J. Cell Biol.* **1991**, *114*, 207.  
 [2] W. G. Dunphy, J. E. Rothman, *Cell* **1985**, *42*, 13.  
 [3] F. Jia, B. Narasimhan, S. Mallapragada, *Biotechnol. Bioeng.* **2014**, *111*, 209.  
 [4] L. Betancor, H. Luckarift, *Biotechnol. Genet. Eng. Rev.* **2010**, *27*, 95.  
 [5] K. S. Rabe, J. Müller, M. Skoupi, C. M. Niemeyer, *Angew. Chem., Int. Ed.* **2017**, *56*, 13574.  
 [6] S. Heintz, A. Mitic, R. H. Ringborg, U. Krühne, J. M. Woodley, K. V. Gernaey, *J. Flow Chem.* **2016**, *6*, 18.  
 [7] A. A. Halim, N. Szita, B. Baganz, *J. Biotechnol.* **2013**, *168*, 567.  
 [8] C. R. Boehm, P. S. Freemont, O. Ces, *Lab Chip* **2013**, *13*, 3426.  
 [9] C. Mukai, L. Gao, J. L. Nelson, J. P. Lata, R. Cohen, L. Wu, M. M. Hinchman, M. Bergkvist, R. W. Sherwood, S. Zhang, A. J. Travis, *Angew. Chem., Int. Ed.* **2017**, *56*, 235.  
 [10] Y. Ono, M. Kitajima, S. Daikoku, T. Shiroya, S. Nishihara, Y. Kanie, K. Suzuki, S. Goto, O. Kanie, *Lab Chip* **2008**, *8*, 2168.  
 [11] S. Fornera, P. Kuhn, D. Lombardi, A. D. Schlüter, P. S. Dittrich, P. Walde, *ChemPlusChem* **2012**, *77*, 98.  
 [12] T. Peschke, M. Skoupi, T. Burgahn, S. Gallus, I. Ahmed, K. S. Rabe, C. M. Niemeyer, *ACS Catal.* **2017**, *7*, 7866.  
 [13] T. Kampe, A. König, H. Schroeder, J. G. Hengstler, C. M. Niemeyer, *Anal. Chem.* **2014**, *86*, 3068.  
 [14] H. Schröder, L. Hoffmann, J. Müller, P. Alhorn, M. Flegler, A. Neyer, C. M. Niemeyer, *Small* **2009**, *5*, 1547.  
 [15] J. R. Kornacki, A. D. Stuparu, M. Mrksich, *ACS Chem. Biol.* **2015**, *10*, 157.  
 [16] M. Mrksich, G. B. Sigal, G. M. Whitesides, *Langmuir* **1995**, *11*, 4383.  
 [17] J. Lee, S.-R. Ryoo, S. K. Kim, J.-H. Ahn, D.-H. Min, W.-S. Yeo, *Anal. Sci.* **2011**, *27*, 1127.  
 [18] C. D. Hodneland, Y.-S. Lee, D.-H. Min, M. Mrksich, *Proc. Natl. Acad. Sci. USA* **2002**, *99*, 5048.  
 [19] J. L. Eisenberg, J. L. Piper, M. Mrksich, *Langmuir* **2009**, *25*, 13942.  
 [20] A. Juillerat, T. Gronemeyer, A. Keppler, S. Gendreizig, H. Pick, H. Vogel, K. Johnsson, *Chem. Biol.* **2003**, *10*, 313.  
 [21] D. Srikun, A. E. Albers, C. I. Nam, A. T. Iavarone, C. J. Chang, *J. Am. Chem. Soc.* **2010**, *132*, 4455.  
 [22] G. Lukinavičius, L. Reymond, K. Johnsson, *Site-Specific Protein Labeling*, Humana, New York **2015**, pp. 107–118.  
 [23] G. V. Los, L. P. Encell, M. G. McDougall, D. D. Hartzell, N. Karassina, C. Zimprich, M. G. Wood, R. Learish, R. F. Ohana, M. Urh, D. Simpson, J. Mendez, K. Zimmerman, P. Otto, G. Vidugiris, J. Zhu, A. Darzins, D. H. Klaubert, R. F. Bulleit, K. V. Wood, *ACS Chem. Biol.* **2008**, *3*, 373.  
 [24] H. N. Chan, Y. Chen, Y. Shu, Y. Chen, Q. Tian, H. Wu, *Microfluid. Nanofluid.* **2015**, *19*, 9.  
 [25] G. Comina, A. Suska, D. Filippini, *Lab Chip* **2013**, *14*, 424.  
 [26] G. H. Seong, J. Heo, R. M. Crooks, *Anal. Chem.* **2003**, *75*, 3161.  
 [27] A. Gong, C.-T. Zhu, Y. Xu, F.-Q. Wang, D. K. Tsabing, F.-A. Wu, J. Wang, *Sci. Rep.* **2017**, *7*, 4309.  
 [28] K. L. Bicker, V. Subramanian, A. A. Chumanevich, L. J. Hofseth, P. R. Thompson, *J. Am. Chem. Soc.* **2012**, *134*, 17015.  
 [29] Y. Elani, R. V. Law, O. Ces, *Nat. Commun.* **2014**, *5*, 5305.  
 [30] O. Hosoya, S. Chono, Y. Saso, K. Juni, K. Morimoto, T. Seki, *J. Pharm. Pharmacol.* **2004**, *56*, 1501.  
 [31] B. Kirby, *Micro- and Nanoscale Fluid Mechanics: Transport in Microfluidic Devices*, Cambridge University Press, Cambridge **2010**, p. 82.  
 [32] T. M. Squires, R. J. Messinger, S. R. Manalis, *Nat. Biotechnol.* **2008**, *26*, 417.  
 [33] J. Fu, M. Liu, Y. Liu, N. W. Woodbury, H. Yan, *J. Am. Chem. Soc.* **2012**, *134*, 5516.  
 [34] Y. Fu, D. Zeng, J. Chao, Y. Jin, Z. Zhang, H. Liu, D. Li, H. Ma, Q. Huang, K. V. Gothelf, C. Fan, *J. Am. Chem. Soc.* **2013**, *135*, 696.  
 [35] M. Mathesh, J. Liu, C. J. Barrow, W. Yang, *Chem. - Eur. J.* **2017**, *23*, 304.  
 [36] a) D.-H. Min, W.-S. Yeo, M. Mrksich, *Anal. Chem.* **2004**, *76*, 3923; b) S. E. Wood, G. Sinsinbar, S. Gudlur, M. Nallani, C.-F. Huang, B. Liedberg, M. Mrksich, *Angew. Chem., Int. Ed.* **2017**, *56*, 16531; c) E. J. Berns, M. D. Cabezas, M. Mrksich, *Small* **2016**, *12*, 3811; d) L. Ban, N. Pettit, L. Li, A. D. Stuparu, L. Cai, W. Chen, W. Guan, W. Han, P. G. Wang, M. Mrksich, *Nat. Chem. Biol.* **2012**, *8*, 769; e) H.-Y. Kuo, T. A. DeLuca, W. M. Miller, M. Mrksich, *Anal. Chem.* **2013**, *85*, 10635.  
 [37] O. I. Wilner, Y. Weizmann, R. Gill, O. Lioubashevski, R. Freeman, I. Willner, *Nat. Nanotechnol.* **2009**, *4*, 249.  
 [38] T. Vong, S. Schoffelen, S. F. M. van Dongen, T. A. van Beek, H. Zuilhof, J. C. M. van Hest, *Chem. Sci.* **2011**, *2*, 1278.  
 [39] K. V. Nguyen, F. Giroud, S. D. Minteer, *J. Electrochem. Soc.* **2014**, *161*, H930.  
 [40] H. Schröder, L. Hoffmann, J. Müller, P. Alhorn, M. Flegler, A. Neyer, C. M. Niemeyer, *Small* **2009**, *5*, 1547.  
 [41] C. M. Niemeyer, J. Koehler, C. Wuerdemann, *ChemBioChem* **2002**, *3*, 242.  
 [42] C. M. Niemeyer, T. Sano, C. L. Smith, C. R. Cantor, *Nucleic Acids Res.* **1994**, *22*, 5530.  
 [43] E. E. Witalison, P. R. Thompson, L. J. Hofseth, *Curr. Drug Targets* **2015**, *16*, 700.  
 [44] T. Zhao, B. Pan, H. B. Alam, B. Liu, R. T. Bronson, Q. Deng, E. Wu, Y. Li, *Sci. Rep.* **2016**, *6*, 36696.  
 [45] A. A. Chumanevich, C. P. Causey, B. A. Knuckley, J. E. Jones, D. Poudyal, A. P. Chumanevich, T. Davis, L. E. Matesic, P. R. Thompson, L. J. Hofseth, *Am. J. Physiol.* **2011**, *300*, G929.

- [46] B. Knuckley, C. P. Causey, J. E. Jones, M. Bhatia, C. J. Dreyton, T. C. Osborne, H. Takahara, P. R. Thompson, *Biochemistry* **2010**, *49*, 4852.
- [47] T. Bennike, K. B. Lauridsen, M. K. Olesen, V. Andersen, S. Birkelund, A. Stensballe, *J. Proteomics Bioinf.* **2013**, *6*, 288.
- [48] A. E. V. Tutturen, A. Holm, M. Jørgensen, P. Stadtmüller, F. Rise, B. Fleckenstein, *Anal. Biochem.* **2010**, *403*, 43.
- [49] V. Chokkalingam, J. Tel, F. Wimmers, X. Liu, S. Semenov, J. Thiele, C. G. Figdor, W. T. S. Huck, *Lab Chip* **2013**, *13*, 4740.
- [50] J. Zhou, J. Zeng, J. Grant, H. Wu, Y. Xia, *Small* **2011**, *7*, 3308.
- [51] G. R. Gossweiler, C. L. Brown, G. B. Hewage, E. Sapiro-Gheiler, W. J. Trautman, G. W. Welshofer, S. L. Craig, *ACS Appl. Mater. Interfaces* **2015**, *7*, 22431.
- [52] A. Rountree, A. Karkamkar, G. Khalil, A. Folch, D. L. Cook, I. R. Sweet, *Heliyon* **2016**, *2*, e00210.
- [53] A. Urrios, C. Parra-Cabrera, N. Bhattacharjee, A. M. Gonzalez-Suarez, L. G. Rigat-Brugarolas, U. Nallapatti, J. Samitier, C. A. Deforest, F. Posas, J. L. Garcia-Cordero, A. Folch, *Lab Chip* **2016**, *16*, 2287.
- [54] K. A. Kilian, M. Mrksich, *Angew. Chem., Int. Ed.* **2012**, *51*, 4891.